Environmental Science & Technology

Article

Cite This: Environ. Sci. Technol. 2017, 51, 13265-13273

pubs.acs.org/est

Gas-Permeable Membrane-Based Conductivity Probe Capable of In Situ Real-Time Monitoring of Ammonia in Aquatic Environments

Tianling Li,[†] Jared Panther,[†,‡] Yuan Qiu,[†,§] Chang Liu,[†,∥] Jianyin Huang,[†,⊥] Yonghong Wu,[#] Po Keung Wong,[¶] Taicheng An,[*,■] Shanqing Zhang,[*,†] and Huijun Zhao[*,†]

[†]Centre for Clean Environment and Energy, Gold Coast Campus, Griffith University, Southport, QLD 4222, Australia

[‡]Goulburn-Murray Water, Tatura, VIC 3616, Australia

[§]Guangxi Vocational and Technical Institute of Industry, 37 Xiuling Road, Nanning, Guangxi 530005, China

[∥]Department of Chemistry, Liaoning Medical University, 40 Songpo Road, Jinzhou, Liaoning 121001, China

[⊥]Division of Information Technology, Engineering and Environment, School of Natural and Built Environment, Mason Lakes Campus, University of South Australia, Adelaide, SA 5095, Australia

[#]State Key Laboratory of Soil and Sustainable Agriculture, Institute of Soil Science, Chinese Academy of Sciences, 71 East Beijing Road, Nanjing, Jiangsu 210008, China

[¶]School of Life Sciences, The Chinese University of Hong Kong, Shatin, NT, Hong Kong SAR, China

[■]Institute of Environmental Health and Pollution Control, School of Environmental Science and Engineering, Guangdong University of Technology, Guangzhou, 510006, China

Supporting Information

ABSTRACT: Aquatic ammonia has toxic effects on aquatic life. This work reports a gas-permeable membrane-based conductivity probe (GPMCP) developed for real-time monitoring of ammonia in aquatic environments. The GPMCP innovatively combines a gas-permeable membrane with a boric acid receiving phase to selectively extract ammonia from samples and form ammonium at the inner membrane interface. The rate of the receiving phase conductivity increase is directly proportional to the instantaneous ammonia concentration in the sample, which can be rapidly and sensitively determined by the embedded conductivity detector. A precalibration strategy was developed to eliminate the need for an ongoing calibration. The analytical principle and GPMCP performance were systematically validated. The laboratory results showed that ammonia concentrations ranging from 2 to 50 000 μg L^{-1} can be detected. The field deployment results demonstrated the GPMCP's ability to obtain high-resolution continuous ammonia concentration profiles and the absolute average ammonia concentration over a prolonged deployment period. By inputting the temperature and pH data, the ammonium concentration can be simultaneously derived from the corresponding ammonia concentration. The GPMCP embeds a sophisticated analytical principle with the inherent advantages of high selectivity, sensitivity, and accuracy, and it can be used as an effective tool for long-term, large-scale, aquatic-environment assessments.

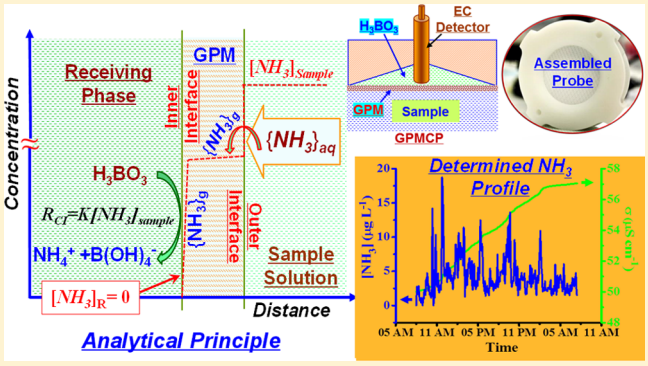

INTRODUCTION

As the third most abundant nitrogen species, ammonia is widely present in aquatic environments. In addition to uncontrollable natural sources, such as the decomposition of organic matter, animal and human wastes, bacterial nitrogen fixation, and atmospheric deposition, aquatic ammonia also comes from agricultural land runoff and municipal discharges.[1−4] Aquatic ammonia can exist in both NH_3 and NH_4^+ forms, and it can transform into other nitrogen species, such as NO_2^-, NO_3^-, and amino acids, through microorganism nitrification processes and living organism assimilation processes.[5,6] Similar to other nitrogen species, elevated concentrations of ammonia in aquatic environments can cause eutrophication, which is a common water pollution phenomenon.[3,7,8] However, in contrast to other aquatic nitrogen species, the presence of ammonia, even at low concentrations, can have direct, toxic effects on aquatic life, leading to adverse ecological consequences.[9−13] With the projected increase in nitrogen fertilizer usage (to boost

Received: July 28, 2017
Revised: October 25, 2017
Accepted: October 25, 2017
Published: October 25, 2017

DOI: 10.1021/acs.est.7b03552
Environ. Sci. Technol. 2017, 51, 13265−13273

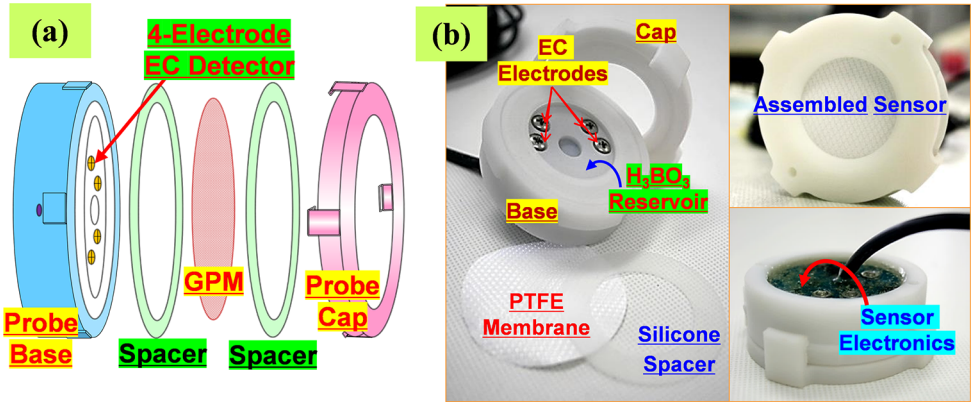

Figure 1. GPMCP configuration and assembly.

agriculture productivity)[14−16] and atmospheric ammonia precipitation (as a result of the increased ammonia emissions from automotive, chemical, and manufacturing industries),[17−21] aquatic ammonia pollution is expected to worsen in the foreseeable future, and this will require effective environmental management practices to mitigate the impact of increased aquatic ammonia pollution.[22,23] In this regard, developing field-based analytical technologies that are capable of in situ real-time monitoring ammonia in a facile and economically viable fashion to enable long-term, large-scale evaluations of aquatic ammonia distribution, migration, and trends will directly benefit environmental management practices.[4,24]

The standard Nessler method is a traditional and widely used laboratory ammonia detection method.[25] This method is a colorimetric-based method with a high sensitivity, but its accuracy can be affected by the presence of metal ions and other nitrogen species.[26−28] Although a number of ammonia flow-injection online detection systems based on automated colorimetric methods have been developed,[29−31] few of these systems have been used for field-based applications due to the high costs for the equipment, installation, operation, and maintenance. Additionally, the inherent reliability and stability issues due to the complex flow-injection system configuration make these systems unsuitable for field-based applications. An ion-selective ammonia electrode is another commonly used ammonia detection method. The electrode possesses an ideal sensor configuration and embodiment for in situ analyses, but it often suffers from insufficient sensitivity and reproducibility. Additionally, and more critically, the electrode only functions under strictly controlled analytical environments that rarely exist in natural environments.[32,33] In an effort to overcome the shortfalls of the colorimetric and electrochemical based online systems, Chow and co-workers developed an elegant micro-distillation flow injection ammonia detection system and successfully applied it to control the chlorination dosage for drinking water treatment.[34,35] They demonstrated that ultra-sensitive detection of ammonia can be achieved by measuring the conductivity changes in a boric acid solution that result from adsorbing ammonia from a water sample via micro-distillation.[36,37] Despite the noticeable advantages of this method, it is not suitable for large-scale, aquatic-environment information collection because of its inability to perform in situ measurements and its complex system configuration. In practice, to meet the needs of large-scale aquatic-environment ammonia assessments, an analytical system should be (i) cheap to build, easy to deploy, low maintenance, and low cost for operation; (ii) highly reliable, sensitive, accurate and interference-free; (iii) capable of in situ measurements without the need for an additional sample delivery system (e.g., pumping system). To date, although different types of ammonia detection methods (e.g., biosensors, fluorescence and chemiluminescence methods) have been reported and successfully used for various applications,[38−43] to the best of our knowledge, none of the reported ammonia detection methods could meet the criteria listed above.

Herein, we report a gas-permeable membrane-based conductivity probe (GPMCP) that meets all the required criteria for long-term, large-scale, in situ, real-time aquatic ammonia monitoring applications. The developed GPMCP innovatively combines a gas-permeable membrane with a homemade, four-point conductivity detector through a small volume of boric acid solution. The probe embeds a simple but effective analytical principle to enable in situ selective ammonia detection (see the Analytical Principle section for details). The simple probe-shaped configuration makes the GPMCP cheap to build and easy to deploy. Unlike the microdistillation flow injection ammonia detection system,[34−37] where the ammonia-containing sample must be pumped into a microboiler and mixed with NaOH to extract the ammonia from the sample, and the extracted ammonia must be condensed and adsorbed before the detection, the GPMCP can directly and continuously extract ammonia from samples through the gas-permeable membrane via a simple neutralization reaction of ammonia with boric acid and simultaneously realize the detection. This unique feature of the GPMCP makes in situ, real-time ammonia monitoring possible. The analytical principles that enable GPMCP to continuously monitor instantaneous ammonia concentrations and determine the average ammonia concentration over a given deployment period are proposed and experimentally validated. A precalibration strategy is also developed to eliminate the need for an ongoing calibration for increased practicality and minimized operational and maintenance costs. The performance of the developed GPMCP is evaluated using synthetic samples and field deployments.

EXPERIMENTAL SECTION

Chemicals, Solutions, and Sample Analysis. All the chemicals used in this work were of AR grade and were purchased from Merck. All the solutions were prepared using deionized water (Millipore Corp., 18 MΩ cm). Sodium hydroxide was used to adjust the testing solution pH. Unless

DOI: 10.1021/acs.est.7b03552
Environ. Sci. Technol. 2017, 51, 13265−13273

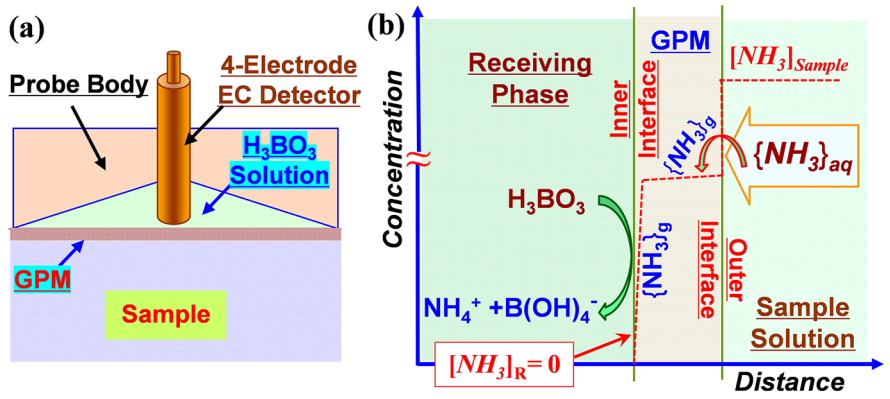

Figure 2. Schematic diagrams illustrating (a) the GPMCP configuration and (b) the conceptual view of the ammonia sensing principle.

otherwise stated, the receiving phase used in this work was 0.500 mol L^{-1} boric acid.

The ammonia nitrogen (NH_3–N) was determined by the APHA Standard Method,[25] where needed, and the standard distillation method was used to achieve sample preconcentration.[25]

Apparatus and Methods. A two-compartment cell (Supporting Information Figure S1) containing 85.0 mL of 0.010 mol L^{-1} HCl and NaCl solutions separated by a PTFE gas-permeable membrane with an exposed area of 1.8 cm^2 was used to investigate the transport of H^+ across the PTFE membrane. A pH electrode was used to monitor the pH change of the NaCl solution.

Figure 1 shows the configuration and assembly of a GPMCP. The probe base consisted of a receiving phase reservoir and a 4-electrode conductivity detector (EC detector). The EC detector was constructed by directly inserting four stainless steel rods (1.5 mm in diameter) into the probe base, and the control electronic circuit board was directly mounted onto the back of the base and fully sealed to ensure it was waterproof. To minimize any electromagnetic interferences, the analog signal generated by the EC detector was in situ converted into a digital signal by the control electronics (Figure 1b). A PTFE membrane purchased from Merck (Fluoropore, pore size 0.22 μm, porosity 85%, diameter 47 mm, thickness 150 μm) was used as the gas-permeable membrane. The GPMCP was assembled by filling the receiving phase reservoir with 2.00 mL of the 0.500 mol L^{-1} boric acid solution and clipping the probe cap onto the base with the PTFE membrane and silicone spacers in between. The exposed PTFE membrane area was 7.07 cm^2.

Figure S2a shows a typical sensing system setup for the laboratory experiments. In addition to the GPMCPs, the system was composed of a data logger (Figure S2b), a wireless data receiver, a control computer, and a sample tank. Each data logger could host up to eight sensors (including temperature and pH sensors). A computer communicated with the data logger for the data transfer/storage and operational control via the wireless data receiver. The control software had an automatic temperature and pH correction function. Two sample tanks with capacities to hold 4 and 25 L of sample solutions were used in this work. Unless otherwise stated, for all the experiments, the temperature and pH sensors were deployed together with the GPMCPs.

Field Deployment. All field deployments were carried out using a self-powered data logger (Figure S2c) that can hold six GPMCPs, one temperature sensor, and one pH sensor and continuously operate for up to 30 days. The data logger was remotely controlled by a computer. Figure S2d schematically illustrates the field deployment of the GPMCPs. The recorded temperature and pH data were used for the data corrections.

For this work, the GPMCPs were deployed at three sites in Gold Coast City, Queensland State in Australia. Site #1 was at the downstream of a creek entrance to the Pacific Ocean, was partially covered by mangroves, and had conductivities that fluctuated between 28 and 45 mS cm^{-1} depending on the tidal actions. Site #2 was located at the upstream of a freshwater creek surrounded by light industry and had an almost constant conductivity of 2.3 mS cm^{-1} that was not affected by tidal actions. Site #3 was a small freshwater lake that was located in an urban residential area and had an almost constant conductivity of 1.3 mS cm^{-1}. During the deployment, water samples were collected every 2 h, preserved at <4 °C, and analyzed for NH_3–N within 12 h in the laboratory.

RESULTS AND DISCUSSION

Analytical Principle. A typical GPMCP contained three key elements: a gas-permeable membrane (GPM), an EC detector, and a boric acid (H_3BO_3) receiving phase (Figure 2a). As illustrated in Figure 2b, when a GPMCP was deployed in an aquatic sample, the dissolved ammonia ($\{NH_3\}_{aq}$) diffused to the outer GPM interface, converted into gas phase ammonia ($\{NH_3\}_g$) at the interface via evaporation and permeated into the GPM. The permeated $\{NH_3\}_g$ inside the GPM rapidly diffused to the inner surface, and $\{NH_3\}_g$ instantaneously and stoichiometrically reacted with H_3BO_3 at the inner GPM interface to produce NH_4^+ and $B(OH)_4^-$ in the receiving phase (eq 1). In effect, the rapidity of this acid–base reaction can efficiently reduce and maintain the concentration of $\{NH_3\}_g$ at the inner GPM surface to essentially zero ($[NH_3]_R \approx 0$) and continuously drive the ammonia transport across the GPM.

$$\{NH_3\}_g + H_3BO_3 \rightarrow NH_4^+ + B(OH)_4^- \quad (1)$$

Considering that ammonia concentrations in most aquatic environments are low (μg L^{-1} to mg L^{-1}), the sensing probe operates under ambient environmental temperatures, and the $\{NH_3\}_g$ ammonia diffuses inside the GPM and reacts with boric acid at the inner GPM interface quickly, it is reasonable to assume that the conversion of $\{NH_3\}_{aq}$ into $\{NH_3\}_g$ at the outer GPM interface is the rate limiting step of the membrane process. Because this conversion process is a continuous, dynamic evaporation process, and for a given GPM, temperature, and deployment time, the rate of $\{NH_3\}_g$ evaporation is

DOI: 10.1021/acs.est.7b03552
Environ. Sci. Technol. 2017, 51, 13265–13273

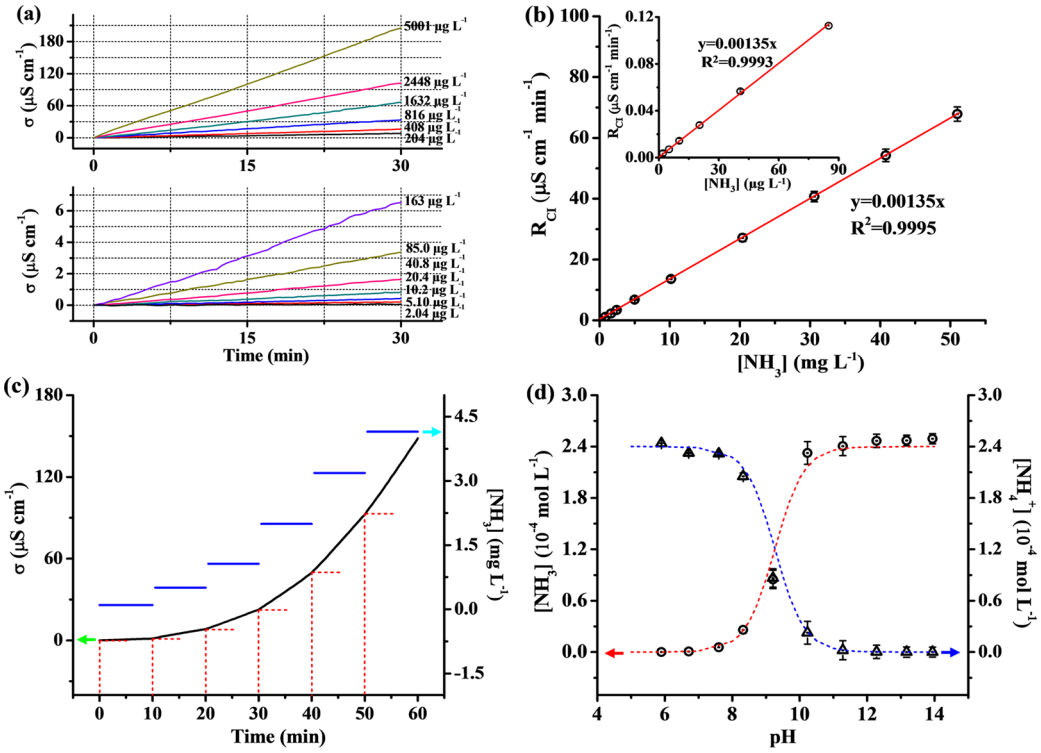

Figure 3. (a) Original σ–t profiles obtained using GPMCP#1 in deployment solutions containing different concentrations of NH_3, (b) R_{CI}–$[NH_3]$ relationship derived from Figures 3a and S3. (c) Original conductivity response obtained from a deployment solution with successively increasing NH_3 concentrations and the corresponding $\overline{[NH_3]}_{sample}$ values (blue lines) determined using eq 6b. (d) The $[NH_3]_{Sample}$ (○) and $[NH_4^+]_{Sample}$ (Δ) values determined using eqs 4 and 7 in a synthetic freshwater deployment solution containing 0.240 μmol L^{-1} of NH_4Cl at different pH values. The red and blue dashed curves show the theoretical distribution of NH_3 and NH_4^+ for the pH values. All the experiments were carried out at 25 °C.

directly proportional to the $\{NH_3\}_{aq}$ concentration in a sample ($[NH_3]_{Sample}$), the flux of ammonia (J) permeating through GPM can be given by

$$J = \frac{d([NH_3]_g)}{dt} = k[NH_3]_{Sample} \quad (2)$$

As the permeated NH_3 from the sample is stoichiometrically converted into NH_4^+ via the interfacial reaction (eq 1), the rate of the NH_4^+ concentration increase in the receiving phase can be expressed as

$$\frac{d([NH_4^+]_R)}{dt} = \frac{J}{V_R} = \frac{k}{V_R}[NH_3]_{Sample} \quad (3)$$

where $[NH_4^+]_R$ is the accumulated NH_4^+ concentration in the receiving phase, and V_R is the volume of the boric acid receiving phase. Because the conductivity of the receiving phase is directly proportional to $[NH_4^+]_R$, the rate of the receiving phase conductivity increase (R_{CI}) can be presented as

$$R_{CI} = \frac{d\sigma}{dt} = \rho\frac{d([NH_4^+]_R)}{dt} = \rho\frac{k}{V_R}[NH_3]_{Sample} = K[NH_3]_{Sample} \quad (4)$$

where ρ is the proportional constant of the EC detector. K depends on the property and exposed area of the GPM, the boric acid receiving phase volume, the characteristics of EC detector, and the deployment temperature. For a given GPMCP with a temperature correction, K is a probe constant that can be readily experimentally determined. That is, the instantaneous ammonia concentration can be determined by simply measuring the R_{CI} of the receiving phase. It is important to note that because K is a probe-specific constant, once the K value of a GPMCP is determined, an ongoing calibration is not required during deployment. This is a distinct advantage for a field-based analytical technique because it reduces the maintenance and operational costs and increases the reliability.[42,44,45]

The ability to determine the average pollutant concentration over a long time period can provide useful information for environmental evaluations and impact predictions.[46] However, for most analytical techniques, determining an average concentration over a prolonged period is not practical because a very high sampling frequency is required and results in a large number of samples and a large assay task and costs. Similar to the diffusive gradients in thin films (DGT) technique,[8,46,47] the GPMCP is also an accumulative method and capable of determining an average concentration over a deployment period. For a given deployment time (t), eq 4 can be rewritten as

$$d\sigma = \rho \bullet d([NH_4^+]_R) = K\int_0^t ([NH_3]_{Sample})dt \quad (5)$$

According to eq 5, the average ammonia concentration ($\overline{[NH_3]}_{sample}$) over a deployment period of t can be determined by

$$\overline{[NH_3]}_{Sample} = \frac{d\sigma}{Kt} \quad (6a)$$

where $d\sigma$ is the total conductivity increment of the receiving phase over the deployment period. $\overline{[NH_3]}_{sample}$ is an absolute

DOI: 10.1021/acs.est.7b03552
Environ. Sci. Technol. 2017, 51, 13265−13273

average concentration because the accumulated $[NH_4^+]_R$ in the receiving phase is the result of the integration of the instantaneous sample ammonia concentrations ($\int_0^t([\overline{NH_3}]_{sample})dt$) over the entire deployment period. For a deployment solution containing a fixed concentration of $\{NH_3\}_{aq}$, eq 6a can be rewritten as

$$[\overline{NH_3}]_{Sample} = \frac{R_{CI}}{K} \quad (6b)$$

NH_3 and NH_4^+ always coexist in aquatic environments. For a given temperature, assuming NH_3 and NH_4^+ are in an equilibrium state, the NH_4^+ concentration in the sample ($[NH_4^+]_{Sample}$) can be calculated from the determined $[NH_3]_{Sample}$ (eq 7)

$$[NH_4^+]_{Sample} = \frac{K_b}{[OH^-]} \times [NH_3]_{Sample} \quad (7)$$

where K_b is the ammonia dissociation base constant.

Analytical Principle Validation. All the validation experiments were performed using the GPMCPs shown in Figure 1 at a constant temperature of 25 °C unless otherwise stated. For all the experiments, a temperature sensor and a pH sensor were deployed with the GPMCPs. For all the conductivity response (σ)−deployment time (t) curves reported in this work, the conductivity data were recorded at a frequency of one reading per minute. Figures 3a and S3 show three sets of original GPMCP σ−t profiles obtained from different $\{NH_3\}_{aq}$ concentrations ranging from 2 μg L^{-1} to 50 mg L^{-1}. Perfect linear curves were observed for all the investigated cases. For each $[NH_3]_{Sample}$, R_{CI} can be derived from the slope of the corresponding σ−t curve. For a given GPMCP and temperature, R_{CI} should be directly proportional to $[NH_3]_{Sample}$, according to eq 4. Figure 3b shows a plot of R_{CI}−$[NH_3]_{Sample}$. As predicted by eq 4, a linear relationship was obtained over the entire $\{NH_3\}_{aq}$ concentration range investigated. It is important to note that the GPMCP probe constant (K) equals the slope of the R_{CI}−$[NH_3]_{Sample}$ curve. The GPMCP used for these experiments had a value of K (25 °C) = 1.35 × 10^{-3} μS cm^{-1} min^{-1} μg^{-1} L (denoted GPMCP#1).

GPMCP#1 was used to obtain a set of conductivity responses from a synthetic freshwater deployment solution with successively increasing NH_3 concentrations (Figure 3c). The blue lines shown in Figure 3c are the corresponding $[\overline{NH_3}]_{Sample}$ determined by eq 6b. Table S1 summarizes the measured R_{CI} values for each investigated $\{NH_3\}_{aq}$ concentration derived from Figure 3c and the $[\overline{NH_3}]_{Sample}$ values determined using eq 6b. If eq 6b is correct, the determined $[\overline{NH_3}]_{Sample}$ values should be equal to the added ammonia concentration. The results show that the deviations between the determined $[\overline{NH_3}]_{Sample}$ values and the added ammonia concentrations are within ±5% for all the investigated cases, and this signifies the validity of eq 6 for determining the absolute average concentration of $\{NH_3\}_{aq}$ over a given deployment period.

A set of experiments was performed to validate eq 7. For all the experiments, 25 L of a synthetic freshwater solution containing 0.240 μmol L^{-1} of NH_4Cl was adjusted to different pH values between 5.90 and 13.94 and was used as the deployment solution. Figure S4 shows the recorded σ−t curves from the deployment solutions with different pH values. The $[NH_3]_{Sample}$ values of the deployment solutions with different pH values were determined using eq 4, and these values were used to calculate the corresponding $[NH_4^+]_{Sample}$ values in accordance with eq 7. Figure 3d shows the plots of both the $[NH_3]_{Sample}$ and $[NH_4^+]_{Sample}$ values against the pH, and the theoretical distributions of $[NH_3]$ and $[NH_4^+]$ with the pH. K_b (25 °C) = 1.75 × 10^{-5} was used for all the calculations. The determined $[NH_3]_{Sample}$ and $[NH_4^+]_{Sample}$ values well agreed with the theoretical values within the pH range from 5.90 to 13.94. Considering the pH range in aquatic environments is normally between 6 and 9, the results shown in Figure 3d confirm that eq 7 is applicable for the determination of $[NH_4^+]$ in aquatic environments. In fact, the $[NH_3]$ and $[NH_4^+]$ in aquatic environments can be simultaneously monitored using eqs 4 and 7, respectively. Furthermore, the absolute average ammonium concentration over a given deployment period ($[\overline{NH_4^+}]_{Sample}$) can be obtained based on the determined $[\overline{NH_3}]_{Sample}$ value in accordance with eq 6.

Sensitivity is important for environmental monitoring applications because the targeted species are often present in low concentrations. The results shown in Figure 3a suggest that the GPMCP is capable of directly determining a concentration of 2 μg L^{-1} of free ammonia. In fact, the sensitivity can be further increased by simply extending the deployment time because the GPMCP is an accumulative method. Additionally, Figure 3b shows an upper linear range of 50 mg L^{-1}, which can be readily extended by reducing the deployment time. Furthermore, the sensitivity, linear range, and maximum deployment time can be tuned by altering the GPMCP design. A GPMCP with a higher ratio of the exposed membrane area to the boric acid receiving phase volume will possess a higher sensitivity with a lower upper linear range and shorter maximum deployment time.

The selectivity is an important performance indicator in many analytical applications, especially for field-based environmental monitoring applications in which the sample matrixes can be highly diverse and complex. The selectivity of the GPMCP was therefore investigated. H^+ was selected as the probing ion because it is the smallest ion in aqueous media. The transport of H^+ across the PTFE membrane was investigated using a two-compartment cell (Figure S1) with 0.010 mol L^{-1} HCl and NaCl solutions separated by a PTFE gas-permeable membrane. Figure S5 shows a typical pH−time profile for the NaCl solution. A measurable decreasing pH trend was not observed over the test period of five days, which means that the transport of H^+ across the membrane did not occur during the test period. This also means that ionic species cannot permeate through the PTFE membrane. This is not a supervising outcome because of the hydrophobic nature of the PTFE membrane. On the basis of the acid−base properties, dissolvable gases in aquatic environments can be classified as neutral (i.e., O_2, N_2, etc.), acidic (i.e., CO_2, H_2S, SO_2, etc.), and basic (i.e., NH_3) gases. According to the GPMCP sensing principle (Figure 2b), only basic gases can continuously permeate through the membrane via the acid−base reaction at the inner membrane interface, but neutral and acidic gases cannot permeate because they do not react with boric acid. To the best of our knowledge, ammonia is the only dissolvable basic gas in aquatic environments with an appreciable solubility. Hence, GPMCP is specific for ammonia detection regardless of the type of aquatic environment, and this is demonstrated in Figure S6 where the determined $[NH_3]_{Sample}$ and $[NH_4^+]_{Sample}$ values in a synthetic seawater matrix over a wide pH range are

DOI: 10.1021/acs.est.7b03552
Environ. Sci. Technol. 2017, 51, 13265−13273

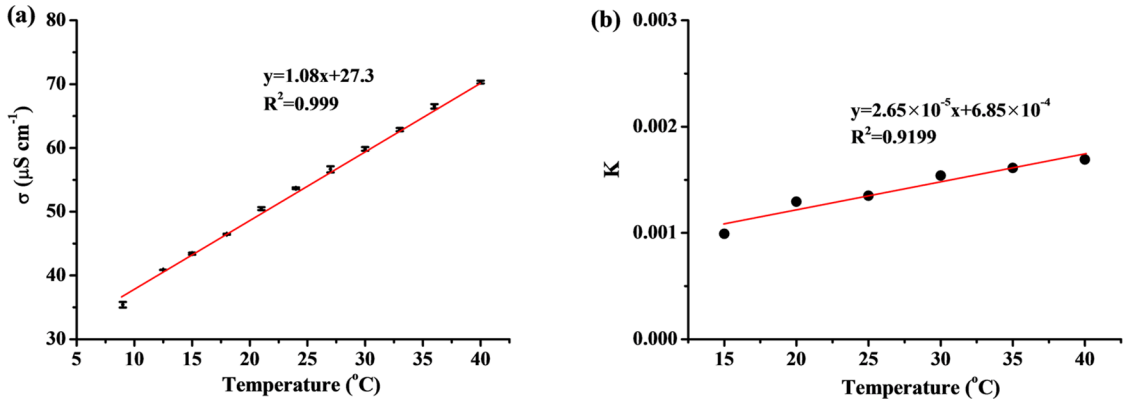

Figure 4. (a) Temperature correction curve for the EC detector in GPMCP#1. (b) Temperature correction curve for the GPMCP#1 constant.

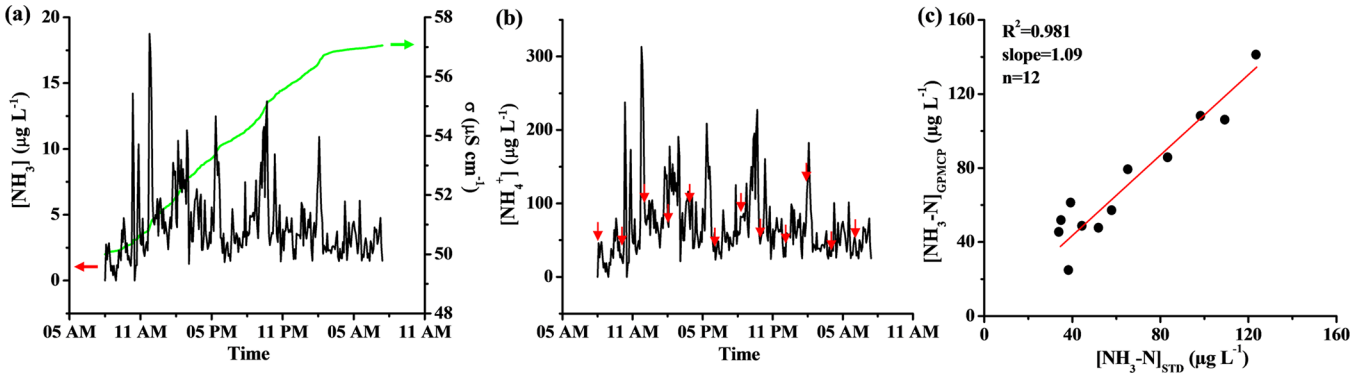

Figure 5. (a) The recorded $\sigma-t$ profile and the corresponding instantaneous NH_3 concentration −time profile. (b) NH_4^+ concentration −time profile (red arrows indicate sampling points for laboratory analysis). (c) Plot of $[NH_3-N]_{GPMCP}$ against $[NH_3-N]_{STD}$.

almost identical to those obtained in a freshwater matrix (Figure 3d).

GPMCP Calibration. An analytical technique that requires no ongoing calibration is highly desirable for field-based environmental monitoring applications. According to eq 4, K is a probe-specific constant. For GPMCP#1, the probe constant at 25 °C was determined to be $K(25\ °C) = 1.35 \times 10^{-3}$ $\mu S\ cm^{-1}\ min^{-1}\ \mu g^{-1}\ L$ (Figure 3b). However, for a given probe, K also depends on the temperature and must be corrected for practical use. A two-step correction strategy was developed for the GPMCP calibration: (i) the temperature effect on the EC detector of the GPMCP was corrected to normalize the conductivities measured at different temperatures (σ_T) to the "standard" conductivity value at 25 °C (σ_{25}); (ii) the σ_{25} data were used to obtain the K−temperature dependent relationship of the GPMCP and to determine the K (T) for practical use.

Figure 4a shows the plots of the measured conductivity changes with the temperatures for GPMCP#1 with a 0.500 mol L^{-1} boric acid receiving phase. The slope and intercept values of 1.08 $\mu s\ cm^{-1}\ °C^{1-}$ and 27.3 $\mu s\ cm^{-1}$ were obtained, respectively. Therefore, the σ_T value at a temperature (T, °C) measured by the EC detector in GPMCP#1 can be converted to σ_{25} by

$$\sigma_{25} = \sigma_T + 1.08 \times (25 - T) \quad (8)$$

.Equation 8 is probe specific and can only be used to correct the EC detector for GPMCP#1. In practice, a temperature correction formula needs to be determined for each probe. In this work, all the measured σ values were real-time corrected to σ_{25} values based on the measured temperature and the predetermined EC detector temperature correction formula (e.g., eq 8) of the probe using the sensor control software. All the conductivity values reported in this work are σ_{25} values unless otherwise stated.

Figure S7 shows six groups of typical $\sigma-t$ curves and the corresponding $R_{CI}-[NH_3]$ curves determined using GPMCP#1 for a set of deployment solutions containing different concentrations of NH_3 at different temperatures between 15 and 40 °C. Each group of the $\sigma-t$ curves was measured at a constant temperature and was used to obtain the R_{CI} values to determine the probe constant ($K(T)$) at the corresponding temperature. The probe constant and temperature dependent relationship can then be determined from the $K(T)-T$ curve shown in Figure 4b:

$$K(T) = 2.65 \times 10^{-5} T(°C) + 6.85 \times 10^{-4} \quad (9)$$

Equation 9 is also probe specific and can only be used to correct the temperature-induced probe constant changes for GPMCP#1. In practice, each GPMCP must be calibrated to obtain the temperature correction equation. Again, the sensor control software automatically corrected for the temperature effect.

In theory, once a GPMCP is calibrated, the obtained probe constant should not change over time, and an ongoing calibration is not needed. Figure S8 shows a set of $\sigma-t$ curves obtained by CPMCP#1 over a period of 142 days in a deployment solution containing 1020 $\mu g\ L^{-1}$ of added NH_3. Over the entire testing period, other than obtaining the results shown in Figure S8, the same probe was used for various other experiments without additional calibration. The determined

DOI: 10.1021/acs.est.7b03552
Environ. Sci. Technol. 2017, 51, 13265−13273

$\overline{[NH_3]}_{Sample}$ values with the probe constant shown in eqs 8 and 9 are almost identical to those for the added NH_3 concentrations, demonstrating that a calibrated GPMCP can be used over a prolonged period without the need for additional calibration. The other GPMCPs (Table S2) used in this work were calibrated using the same method described above.

Field Deployment. GPMCPs were deployed at three sites to evaluate the system performance for field-based monitoring applications. For all the sites, a GPMCP was deployed with a pH probe and a temperature sensor. Site #1 was selected to represent typical estuary waters. GPMCP#1 (see Table S2, $\sigma_{25} = \sigma_T + 1.08 \times (25 - T)$; $K(T) = 2.65 \times 10^{-5}T(°C) + 6.85 \times 10^{-4}$) was deployed at Site #1. During a 24 h deployment period, the conductivity, pH, and temperature of the site water varied between 28−45 mS cm^{-1}, 7.90−8.09, and 21.2−24.8 °C, respectively. These changes were strongly associated with the tidal actions. Higher conductivity and pH values and a lower temperature were observed during the high tide periods. Figure 5a shows the recorded σ−t profile and the corresponding instantaneous NH_3 concentration changes that were determined in real-time using eq 4. The continuous NH_3 concentration profile shows the changes in the NH_3 levels. During the deployment, two high tides occurred at approximately 10 a.m. and 10 p.m., and two low tides occurred at 5 p.m. and 4 a.m. the next day. Higher NH_3 concentrations were observed around these high and low tide points. This could be due to the tidal actions stirring up precipitated NH_3/NH_4^+ in the mangrove wetlands and creek sediments. Furthermore, over the 24 h deployment period, the total conductivity increment ($d\sigma$) derived from Figure 5a was 7.1 μS cm^{-1}, and the absolute average NH_3 concentration ($\overline{[NH_3]}_{Sample}$) of 5.25 μg L^{-1} was obtained from eq 6a. Figure 5b shows the NH_4^+ profile over the deployment period determined by eq 7. The absolute average NH_4^+ concentration ($\overline{[NH_4^+]}_{Sample}$) of 70.3 μg L^{-1} was obtained via eq 7 using $\overline{[NH_3]}_{Sample}$ = 5.25 μg L^{-1}. K_b (25 °C) = 1.75 × 10^{-5} was used for all the calculations. Considering that the temperatures varied between 21.2 and 24.8 °C during the deployment period, the errors introduced by using K_b (25 °C) should be less than 5% because a 5 °C temperature change will cause a <5% change in the K_b value.[48] During the deployment, water samples were collected every 2 h for laboratory determination of the ammoniacal nitrogen ($[NH_3{-}N]_{STD}$) content using a standard method.[25] In our case, the determined $[NH_3{-}N]_{STD}$ was equivalent to the total concentration of NH_3 and NH_4^+. Figure 5c shows a plot of the total NH_3 and NH_4^+ concentrations ($[NH_3{-}N]_{GPMCP}$) determined by GPMCP against $[NH_3{-}N]_{STD}$. The near unity slope value suggests an excellent agreement between the two methods.

Site #2 was selected to represent a typical freshwater creek not affected by tidal actions. GPMCP#2 (see Table S2, $\sigma_{25} = \sigma_T + 1.10 \times (25 - T)$; $K(T) = 5.13 \times 10^{-5}T(°C) + 1.78 \times 10^{-4}$) was deployed at Site #2. During the deployment period, the temperature of the site water varied between 23.5 and 26 °C, and the conductivity (2.3 mS cm^{-1}) and pH (7.57) were nearly constant. In contrast to Site #1, the continuous NH_3 and NH_4^+ concentration profiles (Figures S9a and 9b) recorded over the deployment period showed high NH_3 and NH_4^+ concentrations during the daytime and low concentrations during the night, suggesting that the high daytime NH_3 and NH_4^+ levels could be attributed to discharges into the creek from the surrounding industries. The $\overline{[NH_3]}_{Sample}$, $\overline{[NH_4^+]}_{Sample}$, and average $[NH_3{-}N]_{GPMCP}$ values over the entire deployment period were 5.95, 280, and 286.1 μg L^{-1}, respectively, and the $\overline{[NH_3]}_{Sample}$ and $\overline{[NH_4^+]}_{Sample}$ values during the day (11 a.m. to 6 p.m.) and night (6 p.m. to 8:30 a.m.) varied from 13.21 to 2.22 and 622.7 to 104.9 μg L^{-1}, respectively. The plot of $[NH_3{-}N]_{GPMCP}$ against $[NH_3{-}N]_{STD}$ is given in Figure S9c, and the slope value is near unity, suggesting that the NH_3−N concentrations determined by both methods are essentially the same.

Site #3 was selected to represent immobile water. GPMCP#3 (see Table S2, $\sigma_{25} = \sigma_T + 1.12 \times (25 - T)$; $K(T) = 3.50 \times 10^{-5}T(°C) + 2.85 \times 10^{-4}$) was deployed at Site #3. During the deployment period, the water temperatures varied between 20.6 and 22.5 °C, and the conductivity (1.25 mS cm^{-1}) and pH (6.63) remained almost the same. Figures S10a and b show the NH_3 and NH_4^+ concentration profiles recorded over the deployment period. In a strong contrast to Sites #1 and #2, only trivial variations in the NH_3 and NH_4^+ concentrations were observed over the deployment period. The maximum and minimum NH_3 and NH_4^+ concentrations were 2.48, 1.71 and 1017, 705 μg L^{-1}, respectively. This could be attributed to the immobile nature of the lake. The $\overline{[NH_3]}_{Sample}$, $\overline{[NH_4^+]}_{Sample}$, and average $[NH_3{-}N]_{GPMCP}$ values over the deployment period were 2.11, 865, and 867 μg L^{-1}, respectively. Figure S10c shows the plot of $[NH_3{-}N]_{GPMCP}$ against $[NH_3{-}N]_{STD}$, and the slope value is near unity, confirming the validity of the GPMCP measurement.

The system maintenance requirement is an important practical issue for long-term field-based monitoring applications. In this regard, except periodically replacing boric acid receiving solution, the GPMCP barely requires any other maintenance during long-term deployment.

The above results demonstrate that the GPMCP reported in this work can be used for in situ, real-time monitoring of ammonia and ammonium in aquatic environments in a continuous fashion for a prolonged time period without the need for ongoing calibration. The GPMCP can also be used to easily and conveniently determine the absolute average ammonia and ammonium concentrations over a given deployment period. The GPMCP uses a simple yet sophisticated analytical principle with the inherent advantages of a high selectivity, sensitivity, and accuracy, does not require an ongoing calibration. Additionally, the GPMCP has a simple configuration, and it is cheap to build, easily mass produced, and convenient for field deployment with minimal maintenance. These advantageous features make the GPMCP an effective monitoring tool for long-term, large-scale environmental assessments.

■ ASSOCIATED CONTENT

Supporting Information

The Supporting Information is available free of charge on the ACS Publications website at DOI: 10.1021/acs.est.7b03552.

Figures: Schematic diagram of H^+ permeation experiments; Photographs of ammonia sensing system setup for the laboratory experiments and schematic diagrams of field deployment of the GPMCPs; σ−t profile for high concentrations of $\{NH_3\}_{aq}$; σ−t profile for freshwater deployment solutions with different pH values; pH measurement against time for NaCl compartment; σ−t profile for seawater deployment solutions with different

DOI: 10.1021/acs.est.7b03552
Environ. Sci. Technol. 2017, 51, 13265−13273

pH values and corresponding determined NH_3 and NH_4^+ concentration; $\sigma-t$ curves and corresponding $R_{CI}-[NH_3]$ curves determined using GPMCP#1 at different temperatures; $\sigma-t$ curves obtained using CPMCP#1 over a period of 142 days; Ammonia and ammonium monitoring results for Site #2 and Site #3. Tables: Calculation of R_{CI}, K, and $\overline{[NH_3]}_{Sample}$; Temperature correction for EC detector and GPMCP
(PDF)

AUTHOR INFORMATION

Corresponding Authors

*Tel: +86-20-2388 3536; fax: +86-20-2388 3536; e-mail: antc99@gdut.edu.cn.
*Tel: +61-7-55528155; fax: +61-7-55528067; e-mail: s.zhang@griffith.edu.au.
*Tel: +61-7-55528261; fax: +61-7-55528067; e-mail: h.zhao@griffith.edu.au.

ORCID

Tianling Li: 0000-0002-8185-9698
Jianyin Huang: 0000-0003-1584-9341
Yonghong Wu: 0000-0002-2985-219X
Taicheng An: 0000-0001-6918-8070
Shanqing Zhang: 0000-0001-5192-1844
Huijun Zhao: 0000-0003-3794-4497

Notes

The authors declare no competing financial interest.

ACKNOWLEDGMENTS

We gratefully acknowledge the financial support from Australia Government Flagship Collaboration Research Fund, Sensor Systems for Analysis of Aquatic Environments.

REFERENCES

(1) Bittman, S.; Sheppard, S.; Hunt, D. Potential for mitigating atmospheric ammonia in Canada. *Soil Use Manage.* **2017**, *33* (2), 263−275.
(2) Bash, J. O.; Walker, J. T.; Katul, G. G.; Jones, M. R.; Nemitz, E.; Robarge, W. P. Estimation of in-canopy ammonia sources and sinks in a fertilized Zea mays field. *Environ. Sci. Technol.* **2010**, *44* (5), 1683−1689.
(3) Clarisse, L.; Clerbaux, C.; Dentener, F.; Hurtmans, D.; Coheur, P.-F. Global ammonia distribution derived from infrared satellite observations. *Nat. Geosci.* **2009**, *2* (7), 479−483.
(4) Zhang, X.; Davidson, E. A.; Mauzerall, D. L.; Searchinger, T. D.; Dumas, P.; Shen, Y. Managing nitrogen for sustainable development. *Nature* **2015**, *528* (7580), 51−59.
(5) Denk, T. R.; Mohn, J.; Decock, C.; Lewicka-Szczebak, D.; Harris, E.; Butterbach-Bahl, K.; Kiese, R.; Wolf, B. The nitrogen cycle: A review of isotope effects and isotope modeling approaches. *Soil Biol. Biochem.* **2017**, *105*, 121−137.
(6) Coskun, D.; Britto, D. T.; Shi, W.; Kronzucker, H. J. Nitrogen transformations in modern agriculture and the role of biological nitrification inhibition. *Nat. Plants* **2017**, *3*, 17074.
(7) Qiu, M.; Hu, C.; Liu, J.; Chen, C.; Lou, X. Removal of high concentration of ammonia from wastewater by the ion exchange resin. *Nat. Environ. Pollut. Technol.* **2017**, *16* (1), 261.
(8) Huang, J.; Bennett, W. W.; Welsh, D. T.; Li, T.; Teasdale, P. R. Diffusive Gradients in Thin Films" techniques provide representative time-weighted average measurements of inorganic nutrients in dynamic freshwater systems. *Environ. Sci. Technol.* **2016**, *50* (24), 13446−13454.
(9) Randall, D.; Wood, C.; Perry, S.; Bergman, H.; Maloiy, G.; Mommsen, T.; Wright, P. Urea excretion as a strategy for survival in a fish living in a very alkaline environment. *Nature* **1989**, *337* (6203), 165−166.
(10) Ye, Z.; Wang, S.; Gao, W.; Li, H.; Pei, L.; Shen, M.; Zhu, S. Synergistic effects of micro-electrolysis-photocatalysis on water treatment and fish performance in saline recirculating aquaculture system. *Sci. Rep.* **2017**, *7*, 45066.
(11) Zhou, L.; Boyd, C. E. An assessment of total ammonia nitrogen concentration in Alabama (USA) ictalurid catfish ponds and the possible risk of ammonia toxicity. *Aquaculture* **2015**, *437*, 263−269.
(12) Randall, D.; Tsui, T. Ammonia toxicity in fish. *Mar. Pollut. Bull.* **2002**, *45* (1), 17−23.
(13) Huszár, H.; Pogány, A.; Bozóki, Z.; Mohácsi, Á.; Horváth, L.; Szabó, G. Ammonia monitoring at ppb level using photoacoustic spectroscopy for environmental application. *Sens. Actuators, B* **2008**, *134* (2), 1027−1033.
(14) Webb, J.; Pain, B.; Bittman, S.; Morgan, J. The impacts of manure application methods on emissions of ammonia, nitrous oxide and on crop response—A review. *Agric., Ecosyst. Environ.* **2010**, *137* (1−2), 39−46.
(15) Alexandratos, N.; Bruinsma, J. *World Agriculture Towards 2030/2050: The 2012 Revision*; ESA Working Paper; FAO, Rome, 2012.
(16) Tilman, D.; Cassman, K. G.; Matson, P. A.; Naylor, R.; Polasky, S. Agricultural sustainability and intensive production practices. *Nature* **2002**, *418* (6898), 671−677.
(17) Teng, X.; Hu, Q.; Zhang, L.; Qi, J.; Shi, J.; Xie, H.; Gao, H.; Yao, X. Identification of major sources of atmospheric NH_3 in an urban environment in northern China during wintertime. *Environ. Sci. Technol.* **2017**, *51* (12), 6839−6848.
(18) Sun, K.; Tao, L.; Miller, D. J.; Pan, D.; Golston, L. M.; Zondlo, M. A.; Griffin, R. J.; Wallace, H. W.; Leong, Y. J.; Yang, M. M.; et al. Vehicle emissions as an important urban ammonia source in the United States and China. *Environ. Sci. Technol.* **2017**, *51* (4), 2472−2481.
(19) Sun, K.; Tao, L.; Miller, D. J.; Khan, M. A.; Zondlo, M. A. On-road ammonia emissions characterized by mobile, open-path measurements. *Environ. Sci. Technol.* **2014**, *48* (7), 3943−3950.
(20) Behera, S. N.; Sharma, M.; Aneja, V. P.; Balasubramanian, R. Ammonia in the atmosphere: a review on emission sources, atmospheric chemistry and deposition on terrestrial bodies. *Environ. Sci. Pollut. Res.* **2013**, *20* (11), 8092−8131.
(21) Sapek, A. Ammonia Emissions from Non-Agricultural Sources. *Pol. J. Environ. Stud.* **2013**, *22* (1), 63−70.
(22) Liao, Z. L.; Chen, H.; Zhu, B. R.; Li, H. Z. Analysis and selection of powdered zeolite dosing point in enhanced coagulation−sedimentation for treating micro ammonia polluted raw water. *Desalin. Water Treat.* **2016**, *57* (5), 2142−2151.
(23) Li, Y.; Xu, E. G.; Liu, W.; Chen, Y.; Liu, H.; Li, D.; Liu, Z.; Giesy, J. P.; Yu, H. Spatial and temporal ecological risk assessment of unionized ammonia nitrogen in Tai Lake, China (2004−2015). *Ecotoxicol. Environ. Saf.* **2017**, *140*, 249−255.
(24) Liu, X.; Cheng, S.; Liu, H.; Hu, S.; Zhang, D.; Ning, H. A survey on gas sensing technology. *Sensors* **2012**, *12* (7), 9635−9665.
(25) American Public Health Association, American Water Works Association, Water Environment Federation. *Standard Methods for the Examination of Water and Wastewater*; American Public Health Association (APHA): Washington, DC, USA, 2005.
(26) Jeong, H.; Park, J.; Kim, H. Determination of NH_4^+ in environmental water with interfering substances using the modified Nessler method. *J. Chem.* **2013**, *2013*, 1−9.
(27) Galvão, J. A.; et al. Determination of ammonia in water samples. In *Handbook of Water Analysis*; Nollte, L. M. L., De Gelder, L. S. P., Eds.; CRC Press: Boca Raton, FL, 2013; p 249.
(28) Moliner-Martinez, Y.; Herraez-Hernandez, R.; Campins-Falco, P. Improved detection limit for ammonium/ammonia achieved by Berthelot's reaction by use of solid-phase extraction coupled to diffuse reflectance spectroscopy. *Anal. Chim. Acta* **2005**, *534* (2), 327−334.
(29) Liang, Y.; Yan, C.; Guo, Q.; Xu, J.; Hu, H. Spectrophotometric determination of ammonia nitrogen in water by flow injection analysis

DOI: 10.1021/acs.est.7b03552
Environ. Sci. Technol. 2017, 51, 13265−13273

based on NH_3-o-phthalaldehyde-Na_2SO_3 reaction. *Analytical Chemistry Research* **2016**, *10*, 1−8.
(30) Trojanowicz, M.; Kołacińska, K. Recent advances in flow injection analysis. *Analyst* **2016**, *141* (7), 2085−2139.
(31) Zhu, Y.; Yuan, D.; Huang, Y.; Ma, J.; Feng, S.; Lin, K. A modified method for on-line determination of trace ammonium in seawater with a long-path liquid waveguide capillary cell and spectrophotometric detection. *Mar. Chem.* **2014**, *162*, 114−121.
(32) Melchert, W. R.; Reis, B. F.; Rocha, F. R. P. Green chemistry and the evolution of flow analysis. A review. *Anal. Chim. Acta* **2012**, *714*, 8−19.
(33) Mesquita, R. B. R.; Rangel, A. O. S. S. A review on sequential injection methods for water analysis. *Anal. Chim. Acta* **2009**, *648* (1), 7−22.
(34) Davey, D. E.; McLeod, S.; Chow, C. W.; Ostrowski, J.; Duker, P.; Bustamante, H.; Vitanage, D.; Meli, T. *Development of an On-Line Nitrogen Monitoring System using Microdistillation Flow Analysis*; Intelligent Sensors, Sensor Networks and Information Processing (ISSNIP), Seventh International Conference, 2011; pp 180−183.
(35) Motzko, S.; Fabris, R.; Badalyan, A.; Henderson, R.; Chow, C. W.; Vitanage, D. Assessment of chloramination control strategy based on free-ammonia concentration. *Aqua* **2009**, *58* (1), 29−39.
(36) Lane, R.; Chow, C. K.; Davey, D. E.; Mulcahy, D.; McLeod, S. On-line microdistillation-based preconcentration technique for ammonia measurement. *Analyst* **1997**, *122* (12), 1549−1552.
(37) Chow, C. W.; Lane, R.; Yeow, T.; Davey, D.; Mulcahy, D. Development of an automated flow-injection system for the determination of trace level ammonia. *Lab. Autom. Inf. Manage.* **1997**, *33* (2), 129−136.
(38) Mader, H. S.; Wolfbeis, O. S. Optical ammonia sensor based on upconverting luminescent nanoparticles. *Anal. Chem.* **2010**, *82* (12), 5002−5004.
(39) Liu, F.; Nordin, A.; Li, F.; Voiculescu, I. A lab-on-chip cell-based biosensor for label-free sensing of water toxicants. *Lab Chip* **2014**, *14* (7), 1270−1280.
(40) Chen, H.; Li, H.; Lin, J.-M. Determination of ammonia in water based on chemiluminescence resonance energy transfer between peroxymonocarbonate and branched $NaYF_4$: Yb^{3+}/Er^{3+} nanoparticles. *Anal. Chem.* **2012**, *84* (20), 8871−8879.
(41) Das, T.; Pramanik, A.; Haldar, D. On-line ammonia sensor and invisible security ink by fluorescent zwitterionic spirocyclic meisenheimer complex. *Sci. Rep.* **2017**, *7*, 40465.
(42) Li, T.; Wu, Y.; Huang, J.; Zhang, S. Gas sensors based on membrane diffusion for environmental monitoring. *Sens. Actuators, B* **2017**, *243*, 566−578.
(43) Waich, K.; Mayr, T.; Klimant, I. Fluorescence sensors for trace monitoring of dissolved ammonia. *Talanta* **2008**, *77* (1), 66−72.
(44) Ho, C. K.; Itamura, M. T.; Kelley, M.; Hughes, R. C. *Review of Chemical Sensors for in-Situ Monitoring of Volatile Contaminants*; Sandia Report SAND2001-0643; Sandia National Laboratories: Albuquerque, NM, 2001, pp 1−27.
(45) Hodgkinson, J.; Tatam, R. P. Optical gas sensing: a review. *Meas. Sci. Technol.* **2013**, *24* (1), 012004.
(46) Davlson, W.; Zhang, H. In situ speciation measurements of trace components in natural waters using thin-film gels. *Nature* **1994**, *367* (6463), 546−548.
(47) Davison, W.; Zhang, H. Progress in understanding the use of diffusive gradients in thin films (DGT)−back to basics. *Environ. Chem.* **2012**, *9* (1), 1−13.
(48) Bates, R. G.; Pinching, G. Acidic dissociation constant of ammonium ion at 0 to 50 °C, and the base strength of ammonia. *J. Res. Natl. Bur. Stand.* **1949**, *42*, 419−430.

DOI: 10.1021/acs.est.7b03552
Environ. Sci. Technol. 2017, 51, 13265−13273